Appl Nanosci (2011) 1:165–171
DOI 10.1007/s13204-011-0026-z

ORIGINAL ARTICLE

Quick single-step mechanosynthesis of ZnO nanorods and their optical characterization: milling time dependence

Soumen Dhara · P. K. Giri

Received: 8 June 2011 / Accepted: 23 August 2011 / Published online: 8 September 2011

Abstract We report on the growth of ZnO nanorods (NRs) by a quick single-step mechanochemical process and investigated the milling time dependence on the structural and optical properties of the ZnO NRs. Mechanochemical reactions are carried out in a planetary ball mill for the time durations ranging from 30 min to 5 h. XRD and TEM studies revealed wurtzite structure of the as-grown ZnO NRs with length of several hundreds of nanometers to few micrometers after 30 min of reaction. Average diameter of the as-grown ZnO NRs decreases from 40 to 15 nm with increasing reaction time. Micro-Raman spectra show red-shift in the characteristic Raman modes, indicating presence of milling induced strain. As-grown NRs show blueshift in the excitonic absorption peak with increasing milling time due to decrease in size and induced strain. Room temperature photoluminescence (PL) spectra show strong band-edge related UV emission and other three major emission peaks, two in the UV-blue region and one at the visible region. Post-growth annealing of the as-grown ZnO NRs completely eliminates the defect related visible PL band. Low-temperature PL studies show an additional sharp peak related to donor-bound excitonic transition, revealing the n-type nature of the as-grown NRs.

Keywords ZnO Nanorods · Single-step mechanosynthesis · Photoluminescence · Raman

S. Dhara · P. K. Giri
Department of Physics, Indian Institute of Technology Guwahati, Guwahati 781039, India

P. K. Giri (✉)
Centre for Nanotechnology, Indian Institute of Technology Guwahati, Guwahati 781039, India
e-mail: giri@iitg.ernet.in

Introduction

The past decade has witnessed a considerable volume of research work dedicated to ZnO nanostructures (Özgür et al. 2005). Varieties of nanostructures of ZnO, mainly nanorods (NRs), nanobelts and nanowires have been under intense research attention due to their significant optical and electronic properties.(Li et al. 2008; Giri et al. 2010; Baxter et al. 2006; Lee et al. 2003; Wang 2004a). Optical properties of NRs and nanowires of ZnO are among the most widely studied for exploring their applicability in nanoscale-opto-electronic devices. ZnO is a wide bandgap material (3.4 eV) with a high value of exciton binding energy (60 meV) which makes it a leading opto-electronic material. ZnO is an efficient UV light emitter (Tang et al. 1998; Park et al. 2002) among all other available semiconductor materials. Ultraviolet lasing from ZnO NRs at room temperature, ZnO NRs based dye-sensitized solar cells, photodetectors have been demonstrated (Huang et al. 2001; Baxter et al. 2006; Ahn et al. 2004; Alvi et al. 2010; Chang et al. 2011). Earlier, metal nanoparticles, ZnO nanocrystals and various complex oxide nanoparticles have been synthesized by mechanochemical technique (Tsuzuki and McCormick 2001; Ao et al. 2006; Tsuzuki and McCormick 2004; Pullar et al. 2007). Very recently one-step mechanosynthesis of CdS quantum dots have been reported (Patra et al. 2011). However, no systematic studies are reported on the effect of milling time on the structural and optical properties of the ZnO NRs. Besides, it is an effective method for the growth of nanomaterials and relatively less expensive. For the growth of the NRs by this method a suitable surfactant should be chosen, which play crucial role to grow in one-direction. The important advantages of this method are NRs can be grown at room temperature and a very fast way, compared to any other chemical methods. In addition, sizes of nanorods can be controlled by

reaction time duration and ball to mass ratio. Whereas methods such as vapour–liquid–solid (Wang 2004b) and chemical vapour deposition (Wu and Liu 2002) are high temperature growth ones and formation mechanism of NRs is also a critical one. In the present work, we have synthesized ZnO NRs with various diameters by mechanochemical method at room temperature for reaction time as short as 30 min. The effect of milling time on the structural and optical properties of as-grown and oxygen gas annealed samples are investigated.

Experimental details

For the growth of ZnO NRs, mechanochemical reactions were carried out in a planetary ball-milling apparatus (Retsch, Germany). Zinc acetate [$Zn(CH_3COO)_2$], *N*-cetyl, *N*, *N*, *N*-trimethyl ammonium bromide (CTAB), a cationic surfactant and sodium hydroxide pellets were used as starting materials, which were procured from Sigma-Aldrich, Germany. These materials were first mixed together properly before starting milling process. Millings were performed at 300 rpm for the time durations 30 min, 2 h and 5 h. These samples are named as ZNR-0.5h, ZNR-2h and ZNR-5h, respectively. The ball to starting material mass ratio was kept at a fixed ratio of 10:1. After the mechanochemical reaction, the resultant product was washed several times by DI water (Millipore) and then with alcohol to remove the surfactant and other bi-products. In the next step, it was dried for 2 h at 100°C to remove the water moister and organic agents. To improve the quality of the NRs, annealing was performed at 500°C under oxygen ambient for 1 h to study the structural and optical properties.

The structural and morphological characterizations of the samples were carried out by field emission scanning electron microscopy (FESEM, Zeiss, Sigma) transmission electron microscopy (TEM, JEOL JEM 2100) and X-ray diffraction (Bruker, D8 advance). The optical characterizations were performed using UV–vis spectrophotometer (Varian Carry 50), photoluminescence (PL) spectrometer (thermo electron, AB2) with 325 nm excitation from a xenon lamp and micro-Raman spectrometer (Jobin–Yvon, LabRam 800HR) with a 488 nm Ar laser excitation. Low-temperature PL measurements were done at 80 K with liquid nitrogen as cooling agent using same PL spectrometer.

Results and discussion

FESEM and TEM studies

Morphological characterization by FESEM imaging shows the growth of dense as-grown ZnO NRs. Figure 1 shows the FESEM image of the ZNR-0.5h sample, which clearly shows a bundle of dense ZnO NRs. The inset shows the higher resolution isolated NRs of the same sample. The measured diameter and length of the NRs varies in the range 22–45 and 300–780 nm, respectively. The FESEM images of the ZNR-2h and ZNR-5h samples show similar morphology with smaller lengths in the range 200–600 nm. TEM images of the as-grown samples also confirm the formation of high crystallinity of the ZnO NRs. Figure 2a, b shows the low magnification TEM images of the ZNR-0.5h and ZNR-2h samples. Length and diameter of the NRs for ZNR-0.5h sample varies in the range of 300–800 and 25–40 nm, respectively. With increase in milling time, both diameter and length of the ZnO NRs are decreased due to mechanical milling process. For the ZNR-2h and ZNR-5h, the average diameters of the NRs are $\sim$24 and $\sim$15 nm. The lengths and diameters of the NRs obtained from the TEM images are in close agreement with the FESEM images. Figure 2c shows the high-resolution lattice image taken from one end of single NRs of ZNR-0.5h. The measured lattice spacing is 2.6 Å, which corresponds to the (002) plane. The inset of Fig. 2c shows the electron diffraction pattern of the corresponding NR, which clearly shows the one-dimensional single-crystalline structures.

X-ray diffraction studies

To confirm the crystalline quality and crystalline phase, as-grown ZnO NRs are studied by X-ray diffraction (XRD). The XRD patterns of all the NRs samples shown in Fig. 3 show characteristic peaks of pure hexagonal wurtzite phase of ZnO. It is observed that full width at half maximum (FWHM) of the XRD peaks increase monotonically from ZNR-0.5h to ZNR-5h. It is primarily due to the

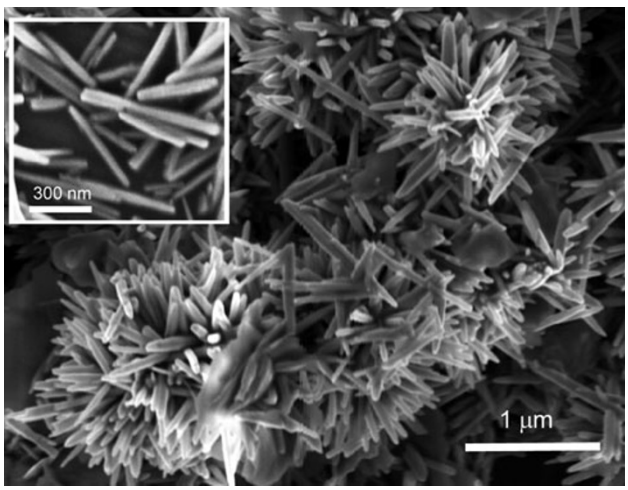

Fig. 1 FESEM image of the ZNR-0.5h sample, where agglomerated bundle of ZnO NRs are clearly visible. *Inset* shows the high-resolution image of the isolated NRs

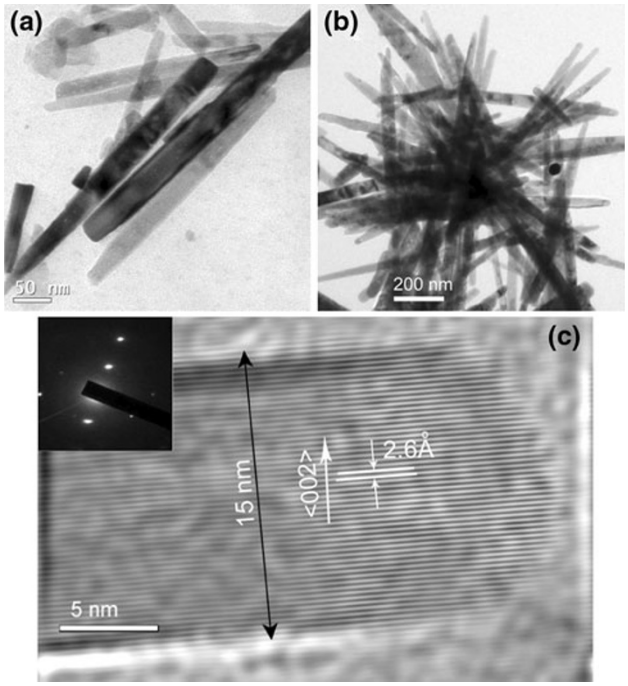

Fig. 2 TEM images of the mechanochemically grown ZnO NRs: **a** ZNR-0.5h and **b** ZNR-2h. **c** High-resolution lattice image of the ZNR-5h. *Inset* shows the SAED pattern of the corresponding NRs, which shows the crystalline hexagonal wurtzite phase

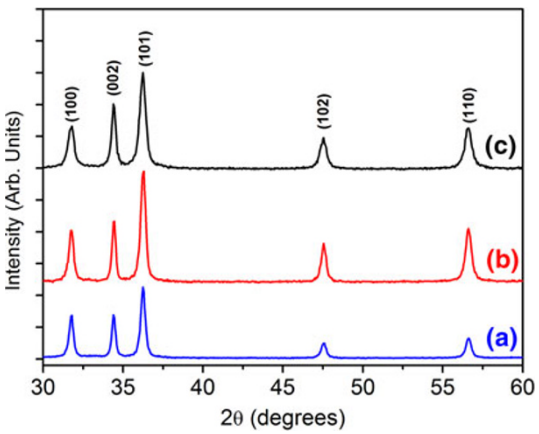

Fig. 3 XRD patterns of the mechanochemically grown ZnO NRs: **a** ZNR-0.5h, **b** ZNR-2h and **c** ZNR-5h

reduction of size of the NRs with increase in milling time. With increasing reaction time, the size of NRs decreases and strain is induced during the milling process. The size reduction primarily contributes to the broadening of XRD line profile. Using Scherrer's formula for calculation of size of NRs ($D = 0.9\lambda/\omega\cos\theta$), we obtain sizes of NRs to be 42, 31 and 25 nm for ZNR-0.5h to ZNR-5h, which closely matches with TEM observations. The lattice strain calculation of these NRs by Williamson–Hall plot (Williamson and Hall 1953) of the XRD line profile shows a decreasing behavior with increase in milling time. This can be explained as follows: in general, milling induces some strain on the system and that gradually increases with milling time. When this strain reached the maximum sustained value, the NRs breaks and released the extra strain and in this way a size reduction is obtained by milling process. XRD patterns of the post-growth annealed samples show highly intense characteristic diffraction peaks of hexagonal phase, which indicates improvement of crystallinity. We also observed a decrease in FWHM of (101) peak, which imply that the NRs recrystallize and strain is released during the annealing process. In our previous study, we observed similar improvement in crystallinity of the 2 h milled samples processed by rapid thermal annealing (Chakraborty et al. 2011).

UV–vis absorption studies

To study the effect of milling time on the bandgap of the mechanochemically grown ZnO NRs, we studied the UV–vis absorption spectra of all the samples, which are shown in Fig. 4. Excitonic absorption peaks are observed at 369, 368 and 365 nm for the ZNR-0.5h, ZNR-2h and ZNR-5h samples, respectively. A clear blueshift in the absorption peak is observed from 369 to 365 nm, as the size reduces from 40 to 15 nm. The observed blueshift is indicative of the increase in bandgap with decrease in size of the NRs. This blueshift with size reduction cannot be attributed fully to quantum size effect in ZnO NRs as these NRs have diameters in the range 15–40 nm, which is much higher than excitonic-Bohr diameter in ZnO (~6.48 nm). Therefore, the change in bandgap is partly contributed by the strain-induced band-widening. After post-growth annealing in oxygen, the absorption peaks are red–shifted

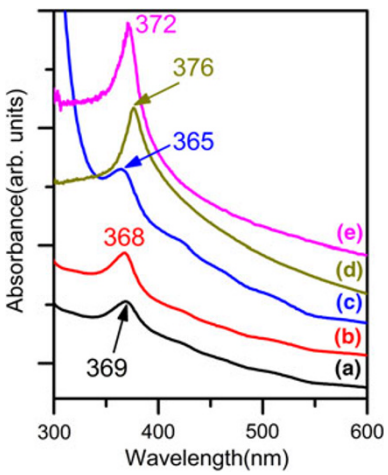

Fig. 4 UV–vis absorption spectra of the mechanochemically grown ZnO NRs: **a** ZNR-0.5h, **b** ZNR-2h and **c** ZNR-5h. **d** and **e** show the spectra for annealed ZNR-0.5h and ZNR-2h samples

to 376 nm for ZNR-0.5h and to 372 nm for ZNR-2h. This indicates relaxation of strain in the ZnO NRs, which is consistent with the XRD and TEM results.

PL studies

Room temperature PL spectra of as-grown and annealed ZnO NRs are shown in Fig. 5. Two major peaks, one UV band and one visible band are observed for all the samples. Each spectrum is fitted with Gaussian peaks and exact values of peak parameters are obtained from fitting. Summary of the fitted peak positions are presented in Table 1. The as-grown NRs show three distinct peaks (1, 2, 3) in the UV–blue region, and one strong, broad peak (4) in the visible region (see Fig. 5a–c). From ZNR-0.5h to ZNR-5h, a blueshift in peak 1 is observed from 379 to 374 nm. This shift is consistent with the results of absorption studies and strain-induced change in band structure is thought to be primarily responsible for the observed blueshift. This UV emission is attributed to free excitonic band-edge recombination (Thonke et al. 2001). The second major peak appears at ~390 nm for all the samples, which originates from the band-to-band transition in the band-tail states of ZnO (Wang et al. 2002). Band tail states are caused by the presence of disorder/defects on the surface of NRs. The peak 3 at ~409 nm is caused by the presence of zinc vacancy related defect states on the surface of the NRs, as reported by Lin et al. (2001) From the PL spectra of the as-grown NRs, it is interesting to note that the relative intensity of the band-edge emission peak (excitonic transition) gradually increase while the intensity of the band-tail related and zinc vacancy related peaks are independent of milling time, which signifies that band-edge related emission becomes dominant with the decrease in size and increase in strain in the NRs.

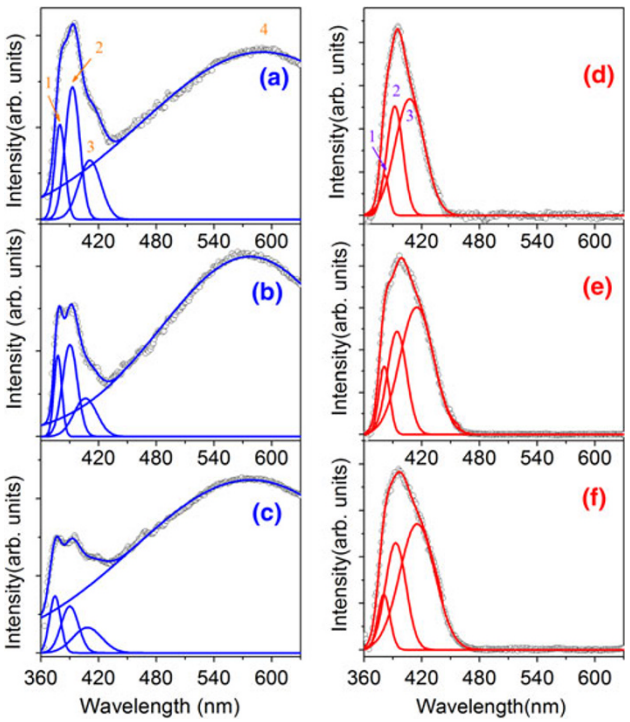

Fig. 5 Room temperature PL spectra of the: **a–c** as-grown and **d–f** annealed, ZNR-0.5h, ZNR-2h and ZNR-5h samples. Deconvoluted individual peaks by Gaussian line shape function are shown in *solid lines* along with resultant fit

Post-growth annealing at 500°C in oxygen ambient results in a redshift of the excitonic band of ~2–6 nm depending on the milling time (see Fig. 5d–f). This is attributed to the relaxation of strain during annealing. On the other hand, peak positions of peak 2 and peak 3 are not affected by annealing. After annealing, a huge enhancement (factor of ~10–30 depending on the milling time) in intensities of PL emission peaks (1–3) and slight change (~0.2–0.8 nm) in FWHM are observed from all the samples. In the visible region, one broad PL band is observed at ~580 nm from all the as-grown NRs. The intensity of this peak is higher for sample with higher reaction time. To confirm the origin of this peak, we performed annealing of the sample at 500°C for 1 h which results in complete elimination of this band. We attribute this visible emission peak in the as-grown samples to the presence of hydroxyl radical on the surface of NRs, which completely desorbs at temperature above 400°C since the desorption rate of hydroxyl radical is maximum at 150°C (Xie et al. 2006). The observation of this particular peak has been reported by Djurisic et al. (2007) for ZnO NRs synthesized by hydrothermal method. In our case, the occurrence of hydroxyl radical on the surface of NRs is likely due to the use of sodium hydroxide, which was used during

Table 1 Summary of the deconvoluted (Gaussian) peak positions of the room temperature PL spectra of different ZnO NRs

Sample	Peak 1 (nm)		Peak 2 (nm)		Peak 3 (nm)		Peak 4 (nm)	
	As-grown	Annealed	As-grown	Annealed	As-grown	Annealed	As-grown	Annealed
ZNR-0.5h	379	381	392	391	409	407	580	–
ZNR-2h	377	380	390	394	408	414	582	–
ZNR-5h	374	380	390	392	408	415	580	–
Peak identity	Bound excitons		Band-tail states		Zinc vacancy		Hydroxyl group	

mechanochemical reaction. Although we dried the as-grown samples at 100°C for 2 h, it may not have removed the OH group completely from surface of the NRs.

To further understand the optical properties of NRs, low-temperature PL measurements of the as-grown ZnO NRs are carried out at 80 K. Experimental data and the deconvoluted PL spectra are shown in Fig. 6. Low-temperature PL reveals a blueshift of 80 meV in the band-edge emission peak with reference to the room temperature PL. Five well-resolved peaks (marked by Roman numbers) are observed in the UV-blue region from all the as-grown NRs samples. The obtained peak positions are located at ~370, ~381, ~390, ~400 and ~409 nm. The first UV peak is assigned to donor-bound excitonic (D°X) transition. Next three peaks are the first-, second-, and third-order phonon replicas of D°X exciton (Fonoberov et al. 2006). The occurrence of the peak at ~409 nm is attributed to zinc vacancy related defects (Lin et al. 2001) states, consistent with the room temperature PL spectra. At room temperature, PL spectra is dominated by free excitonic with emission at ~379 nm (3.27 eV), while at the low temperature the emission for donor-bound excitons becomes dominant and the emission maxima shifts to higher energies. This implies that the as-grown ZnO NRs have donor levels and are of n-type character, despite the fact that no intentional doping is performed during the growth. This is primarily caused by intrinsic defects in ZnO lattice. The absence of deep level emission band around 2.5 eV, which can originate from defects such as Zn_i, V_{Zn}, V_o and O_{Zn} due to poor stoichiometry of ZnO, suggests that the NRs have very few such defects and are of high crystalline quality.

Raman spectra

To check further the crystalline quality of the NRs, Raman scattering measurements were carried out using Ar^+ ion laser of excitation at 488 nm. All the samples show typical Raman spectra with characteristic Raman peaks of hexagonal wurtzite structure, which are shown in Fig. 7. To find out the exact peak positions, all the spectra are fitted with Gaussian function and peak positions are marked in the Raman spectra by dashed lines. For all the samples, the most significant peak with the highest intensity is observed at 436.8, 437.1 and 437.8 cm^{-1} for ZNR-0.5h, ZNR-2h and ZNR-5h, respectively. This particular peak is attributed to the E_2^{high} mode of hexagonal ZnO (Özgür et al. 2005). The occurrence of this peak is due to the vibration of oxygen atoms in ZnO lattice. It also implies that as-grown ZnO NRs are highly crystalline and have wurtzitie structure.

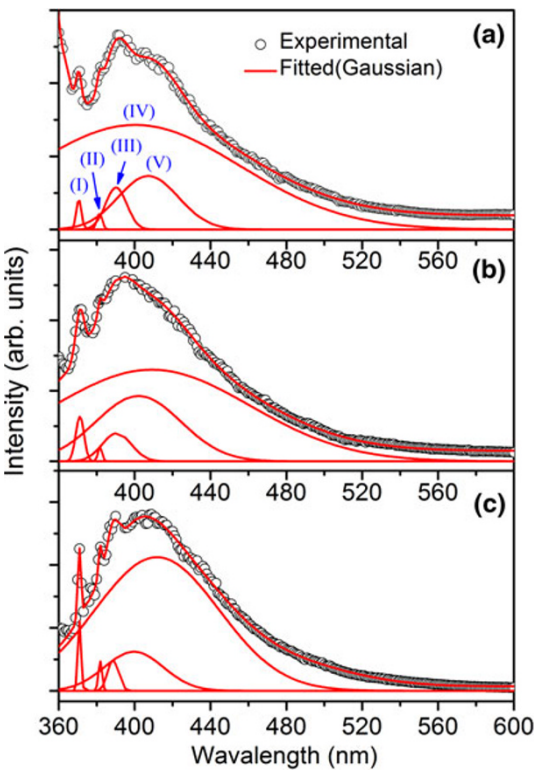

Fig. 6 Low-temperature PL spectra of the as-grown ZnO NRs: **a** ZNR-0.5h, **b** ZNR-2h and **c** ZNR-5h

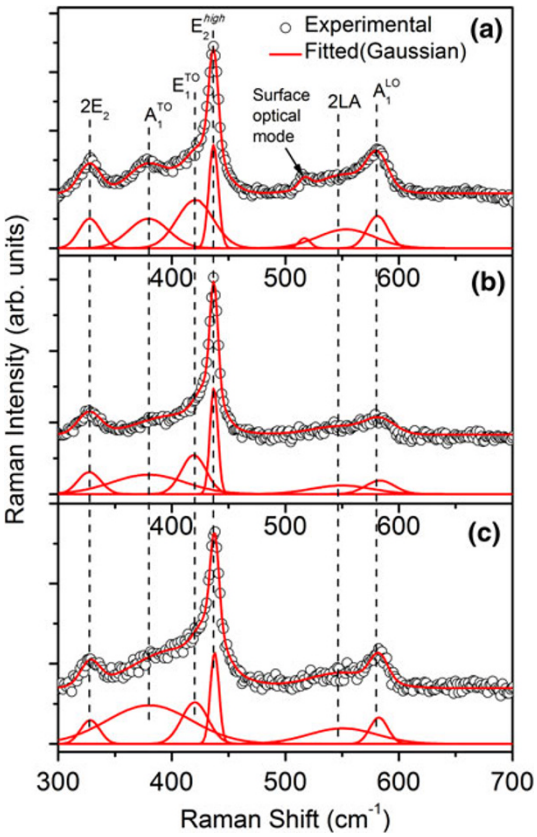

Fig. 7 Raman spectra of the as-grown ZnO NRs : **a** ZNR-0.5h, **b** ZNR-2h and **c** ZNR-5h

Additional Raman modes at ~327, ~379, ~419, ~545 and ~579 cm^{-1} correspond to the $2E_2$, A_1^{TO}, E_1^{TO}, 2LA and A_1^{LO} phonon modes, respectively. Another peak appears at 516 cm^{-1} only for ZNR-0.5h sample, which is due to surface optical phonon mode in ZnO NRs. It is found that E_2^{high} mode of ZNR-0.5h sample are redshifted from that of the strain free ZnO crystals (E_2^{high} at 438 cm^{-1}). Besides the local heating effect during measurement, a major contribution to the redshift comes from the tensile strain present in the as-grown ZnO NRs. The quantum confinement effect is unlikely to affect the Raman modes due to the large size of the NS as compared to exciton-Bohr radius of ZnO. From ZNR-2h to ZNR-5h milled samples, the peak positions are blueshifted and corresponding value of FWHM also increases gradually. This is due to the wider size distribution and release of strain with further milling (Lin et al. 2006). These results are consistent with the XRD results.

Conclusions

We have successfully synthesized uniform ZnO NRs by a quick single-step mechanochemical route and investigated the milling time dependence on the structural and optical properties of the ZnO NRs. XRD and TEM analyses show characteristic wurtzite phase of ZnO NRs. ZnO NRs synthesized by this route show good crystallinity and optical properties. With increasing milling time, average size (diameter) of NRs is reduced from ~40 to ~15 nm. UV–vis absorption spectroscopy shows clear blueshift (369 to 365 nm) in the excitonic absorption peaks. The observed strong UV emission peak in PL spectra is also blueshifted with increasing milling time from 379 to 374 nm. Raman spectroscopy shows very strong E_2^{high} mode for all samples which is the characteristic of wurtzite structure of ZnO. From the measured redshift in Raman spectra, presence of strain is confirmed in the as- grown NRs. Post-growth annealing results in improved crystal structures and it eliminates the defect related visible PL band. Low-temperature PL studies clearly show donor-bound excitonic transitions implying the n-type nature of the as-grown NRs.

References

Ahn SE, Lee JS, Kim H, Kim S, Kang BK, Kim KH, Kim GT (2004) Photoresponse of sol-gel-synthesized ZnO nanorods. Appl Phys Lett 84:5022–5024

Alvi NH, Riaz M, Tzamalis G, Nur O, Willander M (2010) Fabrication and characterization of high-brightness light emitting diodes based on n-ZnO nanorods grown by a low-temperature chemical method on p-4H-SiC and p-GaN. Semicond Sci Technol 25:065004

Ao W, Li J, Yang H, Zeng X, Ma X (2006) Mechanochemical synthesis of zinc oxide nanocrystalline. Powder Technol 168:148–151

Baxter JB, Walker AM, van Ommering K, Aydil ES (2006) Synthesis and characterization of ZnO nanowires and their integration into dye-sensitized solar cells. Nanotechnology 17:S304

Chakraborty R, Dhara S, Giri PK (2011) Effect of rapid thermal annealing on microstructure and optical properties of ZnO nanorods. Int J Nanosci 10:65–68

Chang H, Sun Z, Ho KY, Tao X, Yan F, Kwok WM, Zheng Z (2011) A highly sensitive ultraviolet sensor based on a facile in situ solution-grown ZnO nanorod/graphene heterostructure. Nanoscale Res Lett 3:258–264

Djurisic AB, Leung YH, Tam KH, Hsu YF, Ding L, Ge WK, Zhong YC, Wong KS, Chan WK, Tam HL, Cheah KW, Kwok WM, Phillips DL (2007) Defect emissions in ZnO nanostructures. Nanotechnol 18:095702

Fonoberov VA, Alim KA, A.Balandin A, Xiu F, Liu J (2006) Photoluminescence investigation of the carrier recombination processes in ZnO quantum dots and nanocrystals. Phys Rev B 73:165317

Giri PK, Dhara S, Chakraborty R (2010) Effect of ZnO seed layer on the catalytic growth of vertically aligned ZnO nanorod arrays. Mater Chem Phys 122:18–22

Huang MH, Mao S, Feick H, Yan H, Wu Y, Kind H, Weber E, Russo R, Yang P (2001) Room-temperature ultraviolet nanowire nanolasers. Science 292:1897–1899

Lee JS, Kang M, Kim S, Lee MS, Lee Y-K (2003) Growth of zinc oxide nanowires by thermal evaporation on vicinal Si(100) substrate. J Cryst Growth 249:201–207

Li C, Fang G, Li J, Ai L, Dong B, Zhao X (2008) Effect of seed layer on structural properties of ZnO nanorod arrays grown by vapor-phase transport. J Phys Chem C 112:990–995

Lin B, Fu Z, Jia Y (2001) Green luminescent center in undoped zinc oxide films deposited on silicon substrates. Appl Phys Lett 79:943–945

Lin KF, Cheng HM, Hsu HC, Hsieh WF (2006) Band gap engineering and spatial confinement of optical phonon in ZnO quantum dots. Appl Phys Lett 88:263117

Özgür Ü, Alivov YI, Liu C, Teke A, Reshchikov MA, Dogan S, Avrutin V, Cho SJ, Morkoç H (2005) A comprehensive review of ZnO materials and devices. J Appl Phys 98:041301

Park WI, Kim DH, Jung SW, Yi GC (2002) Metalorganic vapor-phase epitaxial growth of vertically well-aligned ZnO nanorods. Appl Phys Lett 80:4232–4234

Patra S, Satpati B, Pradhan SK (2011) Quickest Single-Step Mechanosynthesis of CdS Quantum Dots and Their Microstructure Characterization. J Nanosci Nanotech 11:4771

Pullar RC, Farrah S, Alford NM (2007) $MgWO_4$, $ZnWO_4$, $NiWO_4$ and $CoWO_4$ microwave dielectric ceramics. J Eur Ceram Soc 27:1059–1063

Tang ZK, Wong GKL, Yu P, Kawasaki M, Ohtomo A, Koinuma H, Segawa Y (1998) Room-temperature ultraviolet laser emission from self-assembled ZnO microcrystallite thin films. Appl Phys Lett 72:3270–3272

Thonke K, Gruber T, Teofilov N, Schonfelder R, Waag A, Sauer R (2001) Donor–acceptor pair transitions in ZnO substrate material. Physica B 308–310:945–948

Tsuzuki T, McCormick PG (2001) ZnO nanoparticles synthesised by mechanochemical processing. Scripta Mater 44:1731–1734

Tsuzuki T, McCormick PG (2004) Mechanochemical synthesis of nanoparticles. J Mater Sci 39:5143–5146
Wang ZL (2004a) Functional oxide nanobelts: Materials, Properties and Potential Applications in Nanosystems and Biotechnology. Annu Rev Phys Chem 55:159
Wang ZL (2004b) Zinc oxide nanostructures: growth, properties and applications. J Phys: Condens Matter 16:R829–R858
Wang QP, Zhang DH, Xue ZY, Hao XT (2002) Violet luminescence emitted from ZnO films deposited on Si substrate by rf magnetron sputtering. Appl Surf Sci 201:123–128
Williamson GK, Hall WH (1953) X-ray line broadening from filed aluminium and wolfram. Acta Metall 1:22–31
Wu JJ, Liu SC (2002) Low-temperature growth of well-aligned ZnO nanorods by chemical vapor deposition. Adv Mater 14:215–218
Xie R, Sekiguchi T, Ishigaki T, Ohashi N, Li D, Yang D, Liu B, Bando Y (2006) Enhancement and patterning of ultraviolet emission in ZnO with an electron beam. Appl Phys Lett 88:134103